

Digital Simulator of the Human Arteries

Jorge Torres Gómez*, Jorge Luis González Rios[†], and Falko Dressler*

*School of Electrical Engineering and Computer Science, TU Berlin, Germany

[†]University of Luxembourg, Luxembourg

torres-gomez@ccs-labs.org, jorge.gonzalez@uni.lu, dressler@ccs-labs.org

Abstract—In supporting healthcare, modeling the human vessels is becoming particularly important due to the potential use of nanosensors in the blood flow. It results in especially important the modeling of pressure and flows along vessels to later predict the dynamic of flowing nanosensors. Supporting this intention, we conceive a digital simulator of the human arteries in this work. Extending widely accepted designs with analog circuits, we provide a low complex design in Simulink/Matlab and suitable to implement in field programmable gate array (FPGA) technology. The findings exhibit a good correspondence of the digital to the original analog design, and the resulted pressure curves behave accordingly to the human standard behavior.

Index Terms—human vessels, arteries, analog circuit, digital design, FPGA

I. INTRODUCTION

Following the paradigm “the body is the network” [1], the human circulatory system (HCS) naturally provides a network connecting through the vessels the various body parts. It is used par excellence to dispense drugs and treat diseases in the body. Advancing this standard procedure, tiny nanosensors are envisioned to travel with the blood flow carrying drugs and targeting diseases at specific regions in the human body [2]. In this area of endeavor, simulators result in handy tools to research the affordability of new conceptions and prototypes. Simulators overcome the natural impediments to conducting experiments in the human vessels on the one hand; on the other hand, they shortcut the cumbersome mathematical models of vessels [3].

Accounting for fluid-dynamics effects in vessels, like laminar flow or turbulences, 3-D models are reported using nanonetwork simulators [4], or numerically evaluating the Navier-Stokes equations for fluids [5], [6]. On the other side, the 0-D models, conceived through electric circuits [6], [7], provide the average flow and pressure (over the geometric coordinates of vessels) while significantly reducing computational resources. The time variable evolution of pressure and flow per vessel segment is directly given as voltages and currents in the electric circuit domain, respectively.

The various reported electric models for the HCS primarily focus on the heart, where only one network models the systemic circulation, or on the arteries as a cascade connection of L and II two ports networks [6]–[9]. Less research is conducted on the complete body accounting for capillaries and veins.

Reported research was supported in part by the project MAMOKO funded by the German Federal Ministry of Education and Research (BMBF) under grant numbers 16KIS0917 and by the project NaBoCom funded by the German Research Foundation (DFG) under grant number DR 639/21-1.

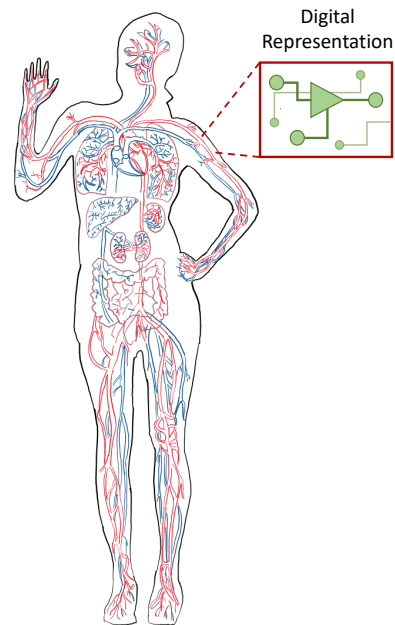


Fig. 1: Digital-circuit model to represent segments of the human arteries.

Mostly, since Rideout [10], just a few works like [11] model the HCS as comprised of a more complete connection of arteries, capillaries, and veins.

In this work, we focus on the electric design for the arteries, given their extended study in the literature detailing the various vessel segments. This paper enhances these previously reported solutions by designing a digital circuit model instead of the typical analog one. In particular, we build upon the work by Noordergraaf et al. [9]. Extending our previous work in [12], we provide a digital design,¹ resulting in an equivalent representation of the vessel segments, as represented in Fig. 1.

When attempting to implement the model as a practical testbed, the digital design introduces numerous advantages in contrast to the analog one using resistors, inductors, and capacitors (as those proposed by Noordergraaf et al. [9] and Rideout [10]). The digital design diminishes the impact of noise in electric circuit implementation, provided it performs just mathematical operations, like adding, multiplying, and delaying. Besides, it typically results in difficulty finding the components for the specific model values when implementing

¹the digital design is publicly accessible at [13]

the analog design in practice. In the digital circuit, the component values are just stored as arrays with an arbitrary accuracy of representation (given by the word and fraction bit length). Furthermore, digital circuits account for flexible designs, where values can be adjusted on the fly. This results particularly advantageous to modeling the live evolution of pressure in vessels with dynamic activities. For instance, that is, from running to walking, and vice versa.

We design the equivalent circuit in the digital domain using blocks for FPGA technology. Departing from the analog electric-circuit design, we apply the bilinear transform to devise the equivalent digital circuit [14],². The implementation is conceived in Simulink/Matlab as detailed in the next two Sections II and III. The resulting design exhibits a good correspondence with the analog one from Noordergraaf et al. [9]. As presented in Section IV, the curves for pressure in the blood vessels also provide a good correspondence with the expected results along the arteries.

II. ANALOG REPRESENTATION OF THE HUMAN ARTERIES

According to the electric circuit models for the human arteries, the vessel can be prototyped in segments where each segment is composed of a connection of resistors, inductors, and capacitors. Fig. 2 illustrates an example in the center body region from the left ventricle in the heart, through the Arcus Aorta down to the Thorax. Each segment implements equal blocks using the L-topology with the resistor and inductor in series (modeling the resistance and the inertia of the blood) and the capacitor as a shunt connection (modeling the compliance of vessels). This diagram was implemented in Simulink/Matlab and is publicly accessible at the repository in [15].

Analytically, the transfer function models this diagram for the analog circuit as

$$H_i^{(a)}(s) = \frac{\frac{1}{sC_i} \parallel Z_{L,i}}{R_i + L_i s + \frac{1}{sC_i} \parallel Z_{L,i}}, \quad (1)$$

in the complex frequency (s) domain [16]. This transfer function not only includes the circuit elements of the given vessel segments (as R_i , L_i , C_i), but also the loading effect from the next blocks, here denoted as $Z_{L,i}$. As depicted in Fig. 3, the load impedance will be in parallel to the shunt capacitor at block i , denoted as the \parallel operator. Besides, the load encompasses one of the following arrangement (c.f. Fig. 2):

- i) a termination resistance (e.g., R_{64});
- ii) the input impedance of a single circuit block k , $Z_{in,k}$, modeling a different vessel segment, or
- iii) the equivalent impedance of the parallel connection of several blocks k_1, \dots, k_n , i.e., $Z_{in,k,1} \parallel \dots \parallel Z_{in,k,n}$.

The Eq. (1) fully describes the input-output voltage relation, yielding the following third-order system after evaluating the equivalent parallel impedance

$$H_i^{(a)}(s) = \frac{b_{1A,i} s + b_{0A,i}}{a_{3A,i} s^3 + a_{2A,i} s^2 + a_{1A,i} s + a_{0A,i}}, \quad (2)$$

²the analog design and digital designs are publicly accessible at [15] and [13], respectively.

where the coefficients based on the nature of the load. In case the load presents an inductive reactance as $Z_{L,i} = R_{L,i} + sL_{L,i}$, the coefficients are

$$\begin{aligned} b_{1A,i} &= L_{L,i}, \\ b_{0A,i} &= R_{L,i}, \\ a_{3A,i} &= C_i L_i L_{L,i}, \\ a_{2A,i} &= C_i L_i R_{L,i} + C_i L_{L,i} R_i, \\ a_{1A,i} &= L_i + L_{L,i} + C_i R_i R_{L,i}, \\ a_{0A,i} &= R_i + R_{L,i}, \end{aligned} \quad (3)$$

in the case the load is a capacitive reactance as $Z_{L,i} = R_{L,i} + \frac{1}{sC_{L,i}}$, then

$$\begin{aligned} b_{1A,i} &= C_{L,i} R_{L,i}, \\ b_{0A,i} &= 1, \\ a_{3A,i} &= C_i C_{L,i} L_i R_{L,i}, \\ a_{2A,i} &= C_i L_i + C_{L,i} L_i + C_i C_{L,i} R_i R_{L,i}, \\ a_{1A,i} &= C_i R_i + C_{L,i} R_i + C_{L,i} R_{K,i}, \\ a_{0A,i} &= 1. \end{aligned} \quad (4)$$

Finally, in the case the load is only resistive as $Z_{L,i} = R_{L,i}$, then

$$\begin{aligned} b_{1A,i} &= 0, \\ b_{0A,i} &= R_{L,i}, \\ a_{3A,i} &= 0, \\ a_{2A,i} &= C_i L_i R_{L,i}, \\ a_{1A,i} &= L_i + C_i R_i R_{L,i}, \\ a_{0A,i} &= R_i + R_{L,i}. \end{aligned} \quad (5)$$

The input impedance $Z_{in,i}$ for each different block is derived based on the transmission matrix representation of the analog RLC circuit as [17]

$$\mathbb{T}_i = \begin{bmatrix} 1 - \omega^2 C_i L_i + j\omega C_i R_i & R_i + j\omega L_i \\ j\omega C_i & 1 \end{bmatrix}, \quad (6)$$

from which we can obtain the input impedance as

$$Z_{in,i} = \frac{\mathbb{T}_i(1,2) + \mathbb{T}_i(1,2) Z_{L,i}}{\mathbb{T}_i(2,2) + \mathbb{T}_i(2,1) Z_{L,i}} \quad (7)$$

where $\omega = 2\pi f$ is the angular frequency, f is the linear frequency, and j is the imaginary unit.

The relation in Eq. (7) allows the evaluation of all the input impedance's from each block recursively. Starting at the terminators, for instance, the Gastrica Sinistra block in Fig. 2 (block RLC_66), where the output impedance is given as the resistor R_{66} , we obtain its input impedance directly using Eq. (7). In the same way, we compute the input impedance for the blocks RLC_64 and RLC_65. Then, after combining the input impedance of the three blocks RLC_64, RLC_65 and RLC_66 (in parallel), we get the output impedance of the Aorta Coelica block (RLC_63). This will provide the value to

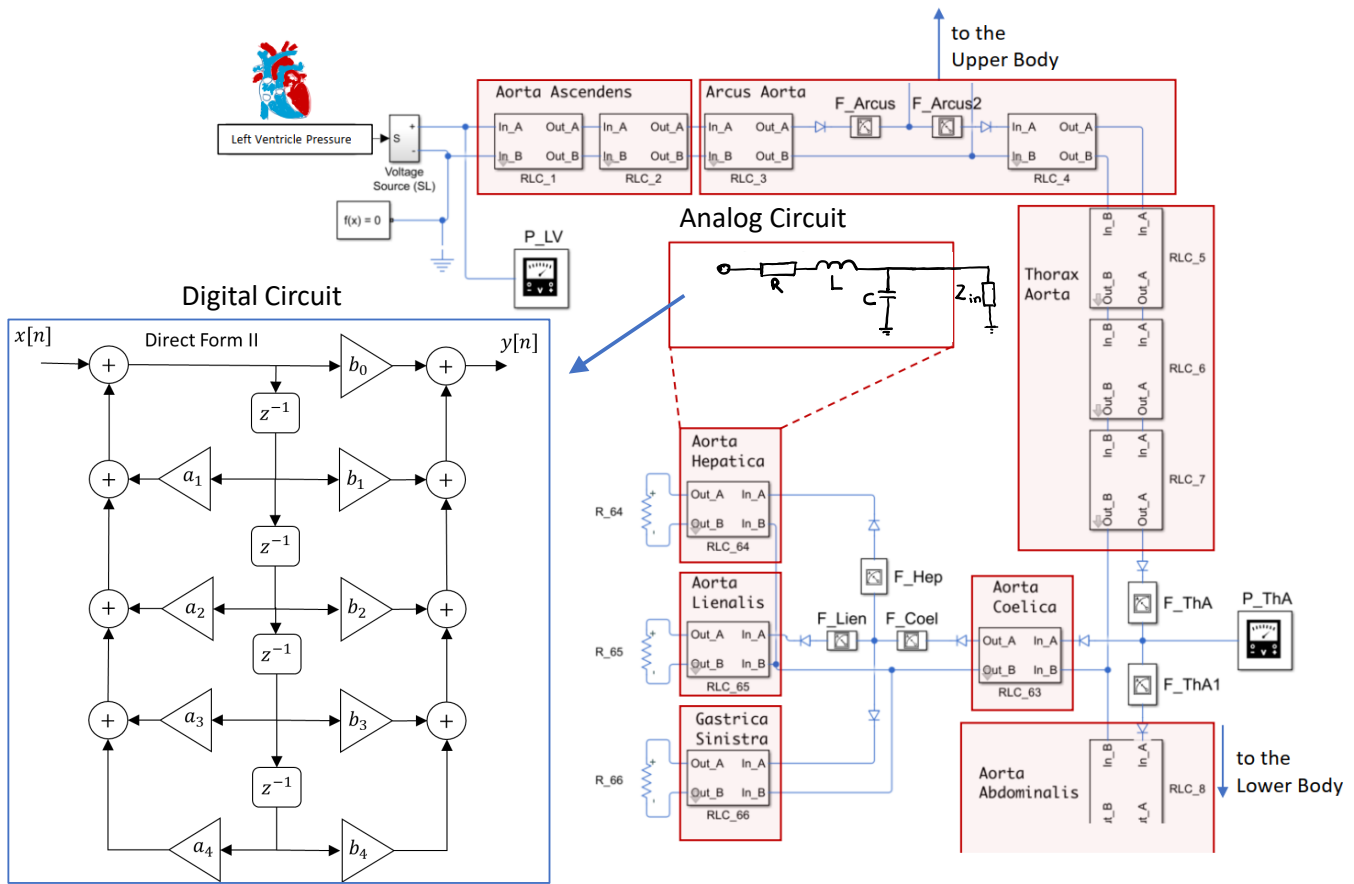


Fig. 2: Design of the human arteries in Simulink.

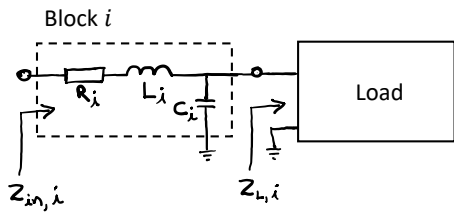


Fig. 3: Output interface in the circuit diagram.

use again the Eq. (7) and evaluate its input impedance. In this way, we gradually compute all the input impedance's block,³

III. DIGITAL REPRESENTATION OF THE HUMAN ARTERIES

Given the analytic representation of the electric circuit as the transfer function in Eq. (1), it directly prototypes as the equivalent digital circuit depicted in Fig. 4 b). The elements in the digital circuit are adders, multipliers, and delay blocks instead of inductors, resistor, and capacitor, where the specific values of the analog parts are mapped as coefficients in the digital circuit. These coefficients (b_i, a_i), used as weights on each branch (as multipliers), are the ones ultimately defining the transfer function in the digital domain.

³the code to evaluate the input impedances is publicly accessible at [13].

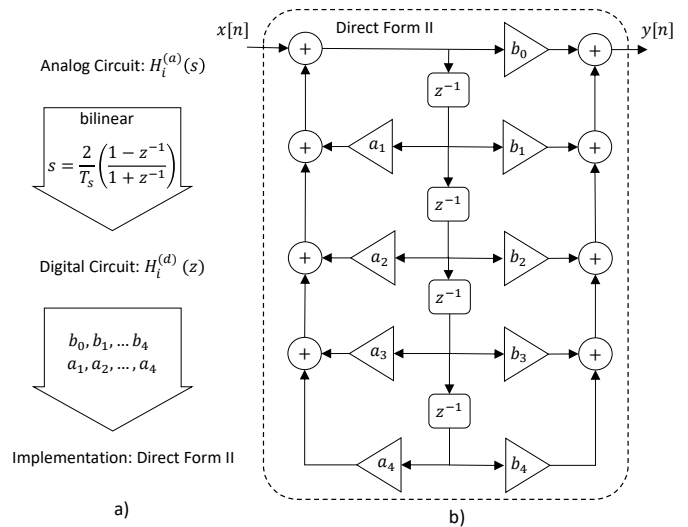


Fig. 4: a) Two-steps methodology to provide the discrete representation of the analog circuits. The implementation is conceived using the direct form II block diagrams in b).

To derive the value of those coefficients, we use the bilinear transformation according to the two-steps methodology, as

depicted in Fig. 4 a) [14]. We depart from the transfer function in the analog domain for each particular vessel segment, as given by $H_i^{(a)}(s)$ in Eq. (1). Then for a sampling period T_s , the bilinear transformation is applied upon the substitution $s = \frac{1}{T_s} \frac{1-z^{-1}}{1+z^{-1}}$ yielding

$$H_i^{(d)}(z) = \frac{b_0 + b_1 z^{-1} + b_2 z^{-2} + b_2 z^{-3}}{a_0 + a_1 z^{-1} + a_2 z^{-2} + a_2 z^{-3}}, \quad (8)$$

as the transfer function in the digital domain. The coefficients are given by

$$\begin{aligned} b_{0,i} &= T_s^2 (2 b_{1A} + T_s b_{0A}) \\ b_{1,i} &= 2 T_s^2 (2 b_{1A} + T_s b_{0A}) - T_s^2 (2 b_{1A} - T_s b_{0A}), \\ b_{2,i} &= T_s^2 (2 b_{1A} + T_s b_{0A}) - 2 T_s^2 (2 b_{1A} - T_s b_{0A}), \\ b_{3,i} &= -T_s^2 (2 b_{1A} - T_s b_{0A}) \\ a_{0,i} &= a_{0A} T_s^3 + 2 a_{1A} T_s^2 + 4 a_{2A} T_s + 8 a_{3A}, \\ a_{1,i} &= 3 a_{0A} T_s^3 + 2 a_{1A} T_s^2 - 4 a_{2A} T_s - 24 a_{3A}, \\ a_{2,i} &= 3 a_{0A} T_s^3 - 2 a_{1A} T_s^2 - 4 a_{2A} T_s + 24 a_{3A}, \\ a_{3,i} &= a_{0A} T_s^3 - 2 a_{1A} T_s^2 + 4 a_{2A} T_s - 8 a_{3A}. \end{aligned} \quad (9)$$

Here we omitted the subscripts (i) for the analog circuit coefficients (b_{kA}, a_{kA}) for the brevity of notation. Using these coefficients, we directly conceive the direct Form II structure as depicted in Fig. 4 b). In this sixth-order structure, the b_i 's are used in the forward branches, while the a_i 's in the backward loops, those implicitly mapping the specific values for resistors, inductors and capacitors from the analog circuit.

Although the digital circuit representation results accurate for a given frequency (in this case 60 Hz from the heart), it does not evaluate the direct component. We remark that the heart's pressure signal also comprises a direct component typically around 60 mmHg, as the pressure typically oscillates in the range 0–120 mmHg.

The digital circuit filters the direct component of the signal because the impedance of inductors and capacitors from the loads are only evaluated for the heart frequency $f_{\text{heart}} = 60$ mHz. Specifically, Eq. (7) evaluates only the specific frequency f_{heart} where the dependency of frequency is explicit in the term ω . Accounting for the direct current component of the heart's signal, we evaluate the circuit response analytically due to its simplicity. For direct components, the circuit behaves only resistive, i.e., all the inductors behave as short-circuits and the capacitor as open-circuits. Therefore, we can use voltage division to evaluate the output voltage from each block based on the direct component of the input as

$$V_{\text{out}} = \frac{R_{L,i}}{R_i + R_{L,i}} V_{\text{in}}, \quad (10)$$

where $R_{L,i}$ is the equivalent load resistance from the next blocks connected at the output. The input resistance of the block i can be simply obtained as

$$R_{\text{in},i} = R_i + R_{L,i}. \quad (11)$$

Starting at the heart, we use Equations (10) and (11) recursively to gradually provide the direct component at the output of each block,⁴

IV. RESULTS

To compare and provide results, we use the analog, and digital implementation designs of the human vessels in [13], [15]. The analog design directly follows the research in [9], where the values for resistors, inductors, and capacitors are summarized in Tables I to III. For the equivalent digital design, we evaluated the coefficients using the methodology in Fig. 4, where the sampling frequency used is 10 times larger than the frequency of the Heart as 60 Hz.

For both designs, we emulate the signal from the heart as a sine wave of frequency 60 Hz in the amplitude range 0–120 mHg. As a future outlook, we will consider a more accurate model. Still, the sine wave representation allows analyzing the two more relevant parameters (pressure and frequency) along the vessels, and conveniently let's examine the circuit from a fasorial representation.

Confirming the equivalence of the digital design, Fig. 5 depicts the transfer function in the Aorta segment as defined by the RLC_1 block. According to this figure, the two circuits match except for the frequencies above the 100 Hz. Although not illustrated here, the other circuit blocks provide the same behavior. In this frequency range, the digital representation of the analog circuit equivalently evaluates the pressure signal from the heart along with the vessel segments.

Regarding the digital circuit, increasing the sampling rate beyond 10 times the frequency of the heart provides a more accurate design. Still, the results illustrate the feasibility of this design in the frequency range below 100 Hz, where the signal coming from the heart is typically located for a person at rest. Designs to account for sports activities, where the frequency of the heart is typically larger than 100 Hz, must provide a more extensive sampling rate.

⁴the matlab code to compute the direct current components is also publicly available at [13]

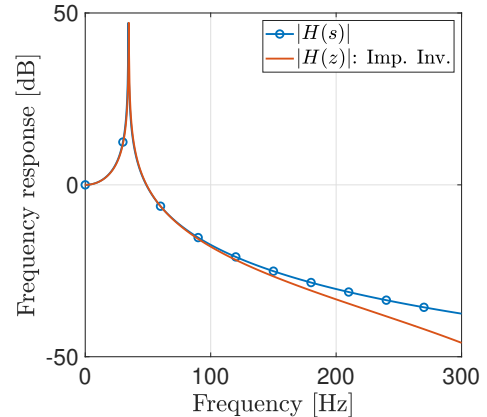


Fig. 5: Frequency response block RLC_disc_1 (Arcus Aorta).

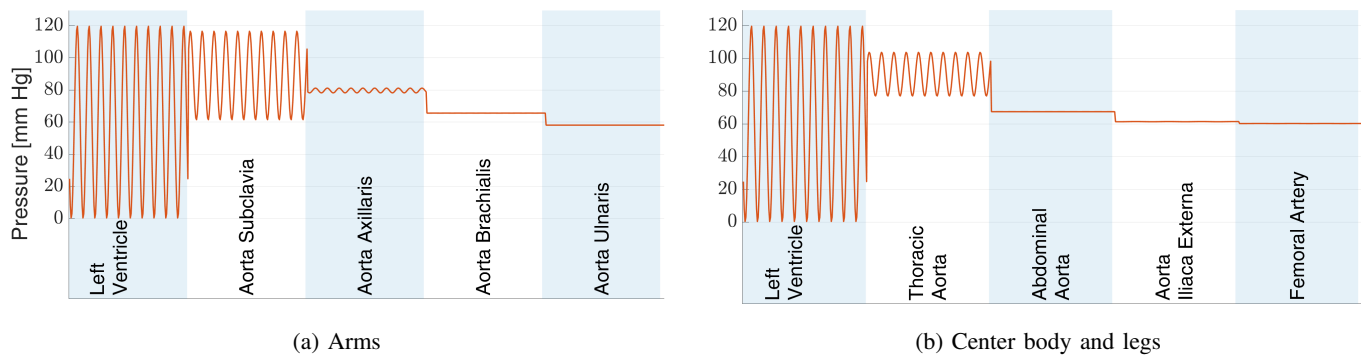


Fig. 6: Resulting blood pressure.

To evaluate the resulting pressure on the vessel segments, Figures 6a and 6b display curves in the arms as well as in the center body and the legs. As expected, the amplitude of elongation is reduced with the increasing distance from the heart, but the average value becomes larger than in the heart (60 mm Hg) for some segments. The increased average will eventually let to expected higher peak amplitudes when using a more accurate model of the heart [18].

V. CONCLUSION

This paper introduces a digital design for the human arteries, publicly accessible, and accounts for the pressure values along with the vessel segments. The design prototypes digital components for FPGA technology, providing a framework for the further modeling of vessels. Advantageously, this model allows analyzing pressure behavior flexibly as long as its parameters can be dynamically reconfigured. We will conduct future research to provide a similar model for the heart, i.e., departing from the reported models with electric circuits, we will prototype the equivalent digital model.

REFERENCES

- [1] S. Sen, S. Maity, and D. Das, "The body is the network: To safeguard sensitive data, turn flesh and tissue into a secure wireless channel," *IEEE Spectrum*, vol. 57, no. 12, pp. 44–49, Dec. 2020.
- [2] U. A. K. Chude-Okonkwo, R. Malekian, B. T. Maharaj, and A. V. Vasilakos, "Molecular Communication and Nanonetwork for Targeted Drug Delivery: A Survey," *IEEE Communications Surveys & Tutorials*, vol. 19, no. 4, pp. 3046–3096, 2017.
- [3] F. v. d. Vosse, "Mathematical modelling of the cardiovascular system," *Journal of Engineering Mathematics*, vol. 47, no. 3/4, pp. 175–183, Dec. 2003.
- [4] R. Wendt and S. Fischer, "MEHLISSA: A Medical Holistic Simulation Architecture for Nanonetworks in Humans," in *7th ACM International Conference on Nanoscale Computing and Communication (NANOCOM 2020)*, Virtual Conference: ACM, Sep. 2020.
- [5] A. Quarteroni, P. Manzoni, and V. M. Vergara, "The cardiovascular system: Mathematical modelling, numerical algorithms and clinical applications," *Acta Numerica*, vol. 26, pp. 365–590, May 2017.
- [6] L. Formaggia, A. Quarteroni, and A. Veneziani, "The circulatory system: from case studies to mathematical modeling," in *Complex Systems in Biomedicine*, A. Quarteroni, L. Formaggia, and A. Veneziani, Eds., Milano, Italy: Springer Milan, 2006, pp. 243–287.
- [7] R. Gul, "Mathematical Modeling and Sensitivity Analysis of Lumped-Parameter Model of the Human Cardiovascular System," PhD Thesis, Fachbereich Mathematik und Informatik, Berlin, Germany, Jan. 2016.
- [8] Y. Shi, P. Lawford, and R. Hose, "Review of Zero-D and 1-D Models of Blood Flow in the Cardiovascular System," *BioMedical Engineering OnLine*, vol. 10, no. 1, p. 33, 2011.
- [9] A. Noordergraaf, P. D. Verdouw, and H. B. Boom, "The use of an analog computer in a circulation model," *Progress in Cardiovascular Diseases*, vol. 5, no. 5, pp. 419–439, Mar. 1963.
- [10] V. C. Rideout, *Mathematical and Computer Modeling of Physiological Systems*. Upper Saddle River, NJ: Prentice Hall, 1991.
- [11] J. Torres Gómez, R. Wendt, A. Kuestner, K. Pitke, L. Stratmann, and F. Dressler, "Markov Model for the Flow of Nanobots in the Human Circulatory System," in *8th ACM International Conference on Nanoscale Computing and Communication (NANOCOM 2021)*, Virtual Conference: ACM, Sep. 2021, 5:1–5:7.
- [12] D. Romanchenko, M. Tartie, B. Que Le, J. Torres Gómez, and F. Dressler, "Molecular Communication Channel Modelling in FPGA Technology," in *International Conference on Networked Systems (NetSys 2021)*, *Workshop on Nanonetworks and Nanocomputation (WoNaN 2021)*, Virtual Conference: EASST, Sep. 2021.
- [13] J. Torres Gómez. "Digital design for the Human Arteries in FPGA." en. (2022), [Online]. Available: <https://www.mathworks.com/matlabcentral/fileexchange/112565-digital-design-for-the-human-arteries-in-fpga> (visited on 06/02/2022).
- [14] A. V. Oppenheim and R. W. Schaffer, *Discrete-time signal processing*, 3rd ed. Upper Saddle River, NJ: Prentice Hall, 2010.
- [15] J. Torres Gómez. "Electric Circuit representation of the Human Arteries." en. (2022), [Online]. Available: <https://www.mathworks.com/matlabcentral/fileexchange/109935-electric-circuit-representation-of-the-human-arteries> (visited on 04/12/2022).
- [16] A. B. Carlson, P. B. Crilly, and J. C. Rutledge, *Communication Systems: An Introduction to Signals and Noise in Electrical Communication*, 4th ed. New York City, NY: McGraw-Hill, 2002, p. 850.
- [17] W. Hayt, J. Kemmerly, J. Phillips, and S. Durbin, *Engineering Circuit Analysis*, 9th ed. New York City, NY: McGraw-Hill Education, 2019.
- [18] A. C. Guyton and M. E. Hall, *Guyton and Hall Textbook of Medical Physiology*, 14th ed. Elsevier, 2015.

TABLE I: Parameters for the analog design of the human arteries (Head and Arms) [9].

Body Region	Artery	RLC block	R[Ω]	L [H]10 ⁻³	C[F]10 ⁻⁹
Head	Carotis Communis	67	22,5	13	8,1
		68	22,5	13	8,1
		69	22,5	13	8,1
		70	11,8	6,85	4,26
		103	22,5	13	8,1
		104	22,5	13	8,1
Arm	Subclavia	71	8,9	6,21	5,8
		72	17,6	12,4	11,6
	Axillaris	73	40,7	18	5,95
		74	37,4	16,5	5,46
	Brachialis	75	105	29	3,61
		76	105	29	3,61
		77	105	29	3,61
		78	76,5	21,2	2,64
		79	373	55,9	1,87
		80	373	55,9	1,87
	Ulnaris	81	373	55,9	1,87
		82	205	30,8	1,03
	Vertebralis	83	625	74,6	1,46
		84	678	80,8	1,58
	Radialis	85	976	94,1	1,13
		86	976	94,1	1,13
		87	976	94,1	1,13
		88	308	29,2	0,349
Interossea Volaris	89	4340	218	0,488	
	90	2360	119	0,266	

TABLE II: Parameters for the analog design of the human arteries (Center Body) [9].

Body Region	Artery	RLC block	R[Ω]	L [H]10 ⁻³	C[F]10 ⁻⁹
Center Body	Ascendens	1	0,0415	0,33	51,9
		2	0,0415	0,33	51,9
	Arcus	3	0,096	0,49	33,2
		4	0,185	0,96	64,4
	Thoracalis	5	0,5	1,83	58,5
		6	0,5	1,83	58,5
		7	0,5	1,83	58,5
		8	0,91	2,48	43,2
		9	0,91	2,48	43,2
	Abdominalis	10	0,91	2,48	43,2
		63	3,82	2,21	1,37
	Coelica	66	625	75,3	1,45
65		105	29	3,61	
Gastrica Sinistra	64	201	41,2	2,58	
	60	63,9	16,2	1,62	
Linealis	61	15,4	10,8	10,1	
	62	687	66,3	0,792	
Hepatica	62	687	66,3	0,792	
	61	15,4	10,8	10,1	
Renalis	60	63,9	16,2	1,62	
	61	15,4	10,8	10,1	
Messentirica Superior	61	15,4	10,8	10,1	
	62	687	66,3	0,792	
Messentirica Inferior	62	687	66,3	0,792	
	61	15,4	10,8	10,1	

TABLE III: Parameters for the analog design of the human arteries (Lower Body) [9].

Body Region	Artery	RLC block	R[Ω]	L [H]10 ⁻³	C[F]10 ⁻⁹
Lower Body	Iliaca Communis	11	7,06	7,23	15,6
		12	18,2	11,5	8,92
	Iliaca Externa	13	7,83	5	3,86
		27	82	25	4,13
	Profundis Femoris	28	82	25	4,13
		29	24,7	7,75	1,24
	Femoralis	14	40,7	18	5,95
		15	40,7	18	5,95
		16	40,7	18	5,95
		17	40,7	18	5,95
		18	47,5	20,9	6,92
		19	88,7	26,7	3,99
	Poplitea	20	88,7	26,7	3,99
		21	88,7	26,7	3,99
		22	373	55,9	1,87
	Tibialis Posterior	23	373	55,9	1,87
		24	373	55,9	1,87
		25	373	55,9	1,87
		26	294	44,2	1,48
	Tibialis Anterior	30	2350	149	0,715
		31	2350	149	0,715
		32	2350	149	0,715
	Tibialis Anterior	33	2350	149	0,715
		34	1350	85	0,41
	Anonyma	35	2,05	2,98	13,6